Acta Pharmaceutica Sinica B 2026;16(8):5070−5085

Chinese Pharmaceutical Association
Institute of Materia Medica, Chinese Academy of Medical Sciences

Acta Pharmaceutica Sinica B

www.elsevier.com/locate/apsb
www.sciencedirect.com

ORIGINAL ARTICLE

H2AC19 promotes lung adenocarcinoma progression *via* p300/EGR1/MMP-1-mediated angiogenesis

Fuwen Zuo[a,b,†], Jinlong Yu[c,†], Tong Liu[a,†], Xiaorui Liu[a,†], Jilong Yin[d], Pengzhong Ding[b], Yuhan Pang[a], Zhengdong Luo[a], Xiaofeng Wang[b], Ling Guo[e], Yirong Zhang[f], Shuang Qi[g], Lutao Du[a], Ziying Wang[b,*], Fan Yi[a,b,*], Xiaoshi Zhang[a,*]

[a]*Department of Clinical Laboratory, National Key Laboratory for Innovation and Transformation of Luobing Theory, Key Laboratory of Cardiovascular Remodeling and Function Research, Chinese Ministry of Education and Chinese Ministry of Health, Qilu Hospital of Shandong University, Jinan 250012, China*
[b]*Department of Pharmacology, School of Basic Medical Sciences, Shandong University, Jinan 250012, China*
[c]*Department of Clinical Pharmacology, The Second Hospital of Shandong University, Jinan 250033, China*
[d]*Advanced Medical Research Institute, Cheeloo College of Medicine, Shandong University, Jinan 250012, China*
[e]*Department of Obstetrics and Gynecology, Qilu Hospital of Shandong University, Jinan 250012, China*
[f]*School of Chinese Language and Literature, Shandong Normal University, Jinan 250014, China*
[g]*Shandong Center for Food and Drug Evaruation and Inspection, Jinan 250014, China*

Received 19 November 2025; received in revised form 2 July 2026; accepted 7 July 2026

KEY WORDS

Lung adenocarcinoma;
Angiogenesis;
H2AC19;
Epigenetic regulation;
Therapeutic target;
EGR1;
MMP-1;
P300

Abstract Angiogenesis is a hallmark of lung adenocarcinoma (LUAD) and a leading cause of mortality. Identifying potential therapeutic targets that modulate this process is of critical clinical importance. Here, we established a 12-gene risk-scoring model through bioinformatics screening and systematically delineated the molecular function of H2AC19, a previously poorly understood histone variant within this signature. Analysis of human LUAD specimens revealed elevated H2AC19 expression, which correlated positively with angiogenesis markers and advanced clinical stage and negatively with patient prognosis. Functional validation using CRISPR/Cas9 in patient-derived organoids (PDOs), *in vitro* cell models and *in vivo* xenografts demonstrated that H2AC19 promotes angiogenesis and tumor growth. Mechanistically, H2AC19 recruits p300 through its amino acid residues 24−88 to specifically augment H3K27 acetylation at the EGR1

*Corresponding authors.
E-mail addresses: histone@126.com (Xiaoshi Zhang), fanyi@sdu.edu.cn (Fan Yi), wangziying@sdu.edu.cn (Ziying Wang).
[†]These authors made equal contributions to this work.
Peer review under the responsibility of Chinese Pharmaceutical Association and Institute of Materia Medica, Chinese Academy of Medical Sciences.

https://doi.org/10.1016/j.apsb.2026.07.010

promoter region, thereby triggering EGR1 transcriptional activation and subsequently promoting MMP-1-driven angiogenesis and progression of LUAD. Furthermore, we evaluated the therapeutic potential of lipid nanoparticles (LNP)-encapsulated siRNA targeting H2AC19, which significantly suppressed angiogenesis and LUAD progression. Collectively, our findings establish a critical role for H2AC19 in governing angiogenesis and highlight its potential as a promising therapeutic target for LUAD.

1. Introduction

Lung cancer remains one of the most prevalent and lethal malignancies worldwide[1]. As the predominant pathological subtype, lung adenocarcinoma (LUAD) accounts for over half of all lung cancer cases and is frequently associated with poor prognosis[2]. Despite substantial advances in diagnostic techniques and therapeutic strategies for LUAD in recent years, the long-term prognosis of LUAD patients remains largely unsatisfactory, highlighting an urgent need to explore new therapeutic targets to improve clinical outcomes[3,4].

Growing research has focused on the role of epigenetic regulation in LUAD progression[5]. As key epigenetic regulators in tumorigenesis, histone variants are paralogs that can replace canonical core histones (H2A, H2B, H3, H4), thereby exerting profound effects on local chromatin structure, DNA accessibility, gene regulation, and DNA damage repair[6−8]. Among all identified histone variants, the H2A family contains the greatest sequence diversity[9]. Studies have implicated genetic alterations in H2A variant-encoding genes in carcinogenesis, and accumulating evidence supports their potential as pivotal prognostic indicators or biomarkers for cancer detection and therapeutic intervention[10].

H2AC19 is a new member of the H2A family, which is mapped to chromosome 1q21 and encoding a 130-amino-acid protein in humans (GeneCards database). Limited bioinformatics evidence indicates that H2AC19 expression is regulated and in response to diverse infectious and various therapeutic regimens, including chemotherapy and traditional Chinese medicine, implying its potential functional involvement in disease pathogenesis and drug responsiveness[11-13]. Nevertheless, its precise biological functions, underlying regulatory pathways, and translational clinical potential remain largely uncharacterized.

In this study, we found that H2AC19 was significantly upregulated in LUAD and promoted tumor progression in both *in vitro* and *in vivo* models. We further demonstrated a hitherto unreported role of H2AC19 in modulating angiogenesis *via* the p300/EGR1/MMP-1 pathway, illustrating the potential of the LNP/si-H2AC19 complex as a promising therapeutic approach for LUAD treatment. Our findings highlight the potential of H2AC19 as both a prognostic biomarker and an innovative therapeutic target in LUAD.

2. Materials and methods

Details for the materials and methods are presented in the Supporting Information.

2.1. Animal studies

All animal procedures were conducted following ethical approval (IACUC-QHSU, KYLL-2024(ZM)-1085) and adhered to National Institutes of Health (NIH) guidelines for laboratory animal welfare. Male BALB/c nude mice (6 weeks old) were purchased from Beijing Vital River Laboratory Animal Technology Co., Ltd. (China) and housed under specific pathogen-free (SPF) conditions. Randomization and blinding were implemented during group allocation, surgical interventions, and outcome assessments. For tumorigenesis, a suspension of 10^7 cells/mL was subcutaneously injected into the right dorsal flank of nude mice. Upon reaching humane endpoints, the mice were euthanized under deep anesthesia, and tumors were excised, weighed, and documented.

2.2. LUAD PDO culture

Organoids were established as previously described[14]. In brief, fresh tissue samples were processed immediately after surgical resection. The minced specimens were incubated in 5 mL digestion buffer containing collagenase B and DNase I at 37 °C with gentle agitation for 30−60 min. The cell suspensions were subsequently filtered and centrifuged, and the pellets were embedded in Matrigel (Corning, Tewksbury, MA, USA) in 24-well plates. PDOs were cultured at 37 °C with 5% CO_2 in a humidified incubator, and the medium was changed three times weekly.

2.3. Gene knockout (KO) using the CRISPR/Cas9 system

CRISPR plasmids (Santa Cruz) were transfected into A549/H1299 cells using UltraCruz reagent according to the manufacturer's protocol. Cas9/sgRNA constructs targeting H2AC19 (or MMP-1, EGR1) constructs were introduced into cells seeded in 6-well plates for 12 h. Transfection efficiency was confirmed by GFP expression. Cells were subjected to 14 days of puromycin (0.5 μg/mL) selection. GFP-positive single clones were expanded from 96-well plates, with H2AC19 (or MMP-1, EGR1) protein levels were assessed by Western blot. The genomic sequencing data for the target gene deficient A549 and H1299 cells are showed in Supporting Information Fig. S1.

2.4. Tube formation assay

Matrigel (250 μL/well, BD) was added to 24-well plates and allowed to polymerized at 37 °C for 30 min. HUVECs (2×10^5 cells/well) were seeded and incubated in conditioned medium for 8 h. Node counts per well were quantified in triplicate.

2.5. Chicken chorioallantoic membrane (CAM) assay

CAM assay was performed at the eighth day of fertilized chicken eggs referring to the methods according to previous studies[15]. In brief, a 1.0-cm window was opened in the air sac and the underlying shell membrane was removed to expose the CAM. A 0.5-

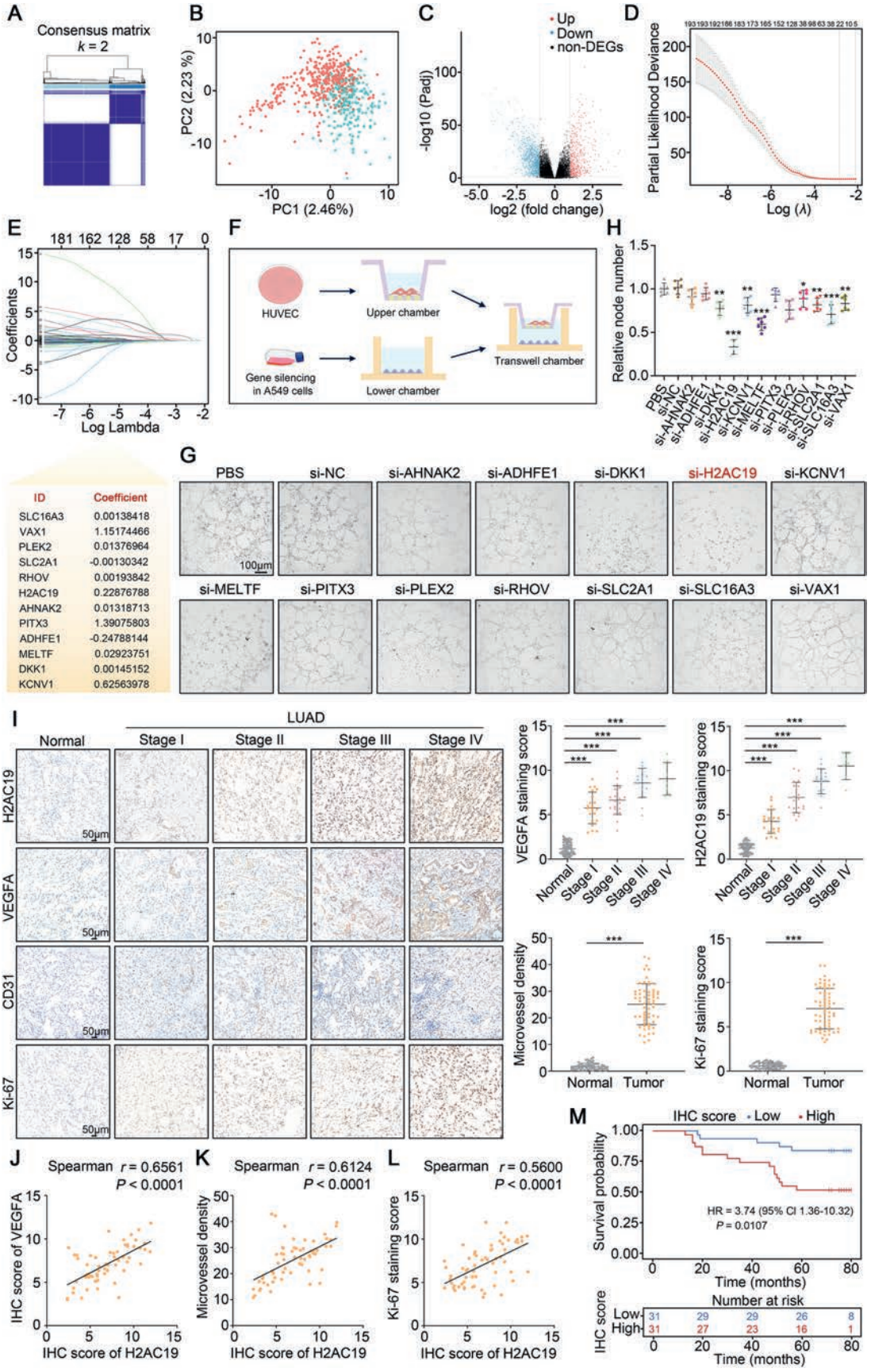

Figure 1 Upregulation of H2AC19 is associated with poor prognosis of patients with LUAD. (A) Heatmap showing the sample clustering at consensus "$k = 2$". (B) PCA analysis indicating an obvious difference in transcriptomes between the two subgroups. (C) Volcano plot of

cm filter paper disc was placed on the CAM and treated with 100 μL of fresh lung cancer cell-conditioned medium. The eggs were sealed and incubated at 37.8 °C (60%−80% humidity) for 5 days. CAM images (Canon camera) analyzed *via* Image View 3.7 software were used to assess vascular responses through vessel count comparisons with controls.

2.6. Real-time polymerase chain reaction (qPCR)

Total RNA was extracted with TRIzol reagent (Invitrogen). The mRNA expression levels were determined by real-time qRT-PCR using a Bio-Rad iCycler system (Bio-Rad, Hercules, CA, USA). The sequences of specific primers are listed in Supporting Information Table S1.

2.7. Western blot analysis

Total protein was extracted from cells using RIPA lysis buffer, separated by SDS-PAGE, and transferred to PVDF membranes. After blocking with 5% skim milk, membranes were incubated with primary antibodies. Antibodies used in this study are summarized in Supporting Information Table S2. Band intensity was quantified by Image J software normalized to housekeeping protein.

2.8. RNA interference and plasmid transfection

Cells were cultured in antibiotic-free medium. siRNAs targeting AHNAK2, ADHFE1, DKK1, H2AC19, KCNV1, MELTF, PITX3, PLEK2, RHOV, SLC2A1, SLC16A3, VAX1 and scramble control, as well as EGR1/MMP-1 overexpression plasmids and corresponding empty vectors, were transfected into cells using Lipofectamine 3000 (Invitrogen) following the manufacturer's protocol. The sequences of siRNA oligonucleotides are listed in Supporting Information Table S3.

2.9. Statistics

Data are expressed as means ± SD. Statistical analysis were performed with GraphPad Prism (version 8.0, GraphPad Software, San Diego, CA, USA). Details for statistics can be found in the Supporting Information.

3. Results

3.1. Construction and validation of a risk score model based on 12 core genes for LUAD prognosis

Given the critical role of hypoxia microenvironment and angiogenesis in tumor progression[16], we analyzed LUAD transcriptomic data from The Cancer Genome Atlas (TCGA) database using the HALLMARK-HYPOXIA and HALLMARK-ANGIOGENESIS gene sets from the Molecular Signatures Database (MSigDB). Based on consensus clustering analysis of 233 hypoxia and angiogenesis associated genes (Supporting Information Table S4), we identified two stable LUAD subgroups in the TCGA-LUAD cohort, with principal component analysis (PCA) confirming distinct transcriptional separation (Fig. 1A and B). Subsequently, differential expression analysis between the two subgroups revealed 1573 differentially expressed genes, of which 554 were upregulated and 1019 downregulated (Fig. 1C). After univariate Cox regression analysis, we screened 12 prominent genes using LASSO regression and calculated the coefficient of each gene in the risk-scoring formula *via* multivariate Cox regression. Finally, a 12-gene signature model was constructed and used to classify patients into high-risk and low-risk group (Fig. 1D and E). In the TCGA-LUAD cohort, high-risk patients defined by this signature exhibited significantly poorer overall survival, with time-dependent AUC values of 0.699, 0.714, and 0.683 for 1-, 3-, and 5- year survival, respectively (Supporting Information Fig. S2A and S2B). We then validated the prognostic performance of this model in two independent cohorts, GSE31210 and GSE50081, where high-risk patients consistently presented inferior survival outcomes (Fig. S2C−S2F). Importantly, we successfully constructed a well-calibrated nomogram composed of the signature risk score and multiple clinicopathological features for predicting the survival time of LUAD patients, which demonstrated strong predictive accuracy (5-year C-index: 0.991, Fig. S2G). Decision curve analysis indicated that the model conferred a substantial clinical benefit across a wide range of thresholds probabilities (Fig. S2H). Moreover, we compared the predictive performance of our constructed 12-gene signature with previously published prognostic models related to hypoxia and angiogenesis across three independent cohorts. Time-dependent ROC analyses revealed that our model achieved comparable or superior AUC values at 1-, 3-, and 5-year time points compared with most existing signature models, and showed better prediction performance at 3- and 5-year time points (Supporting Information Table S5 and Fig. S2I).

3.2. Upregulation of H2AC19 is associated with poor prognosis in LUAD patients

Furthermore, we examined the expression patterns of 12 core genes in paired tumor and normal tissues (Fig. S2J), confirming that most genes were upregulated in LUAD tissues. To verify their functions, we silenced these genes in A549 cells (Fig. S2K) and established an indirect co-culture system using Transwell

angiogenensis and hypoxia genes in TCGA database. Red and blue nodes indicate upregulated and downregulated genes, respectively. (D) Cross validation for tuning parameter selection in the LASSO regression. (E) LASSO coefficient profiles and corresponding coefficient of 12 candidate genes. (F) Schematic diagram of lung adenocarcinoma cells co-cultured with HUVEC cells. (G, H) Tube formation assay of HUVECs treated for 48 h with conditioned medium (CM) from A549 cells under different conditions. Scale bar = 100 μm. (I) Representative immunohistochemistry of H2AC19, VEGFA, CD31 and Ki-67 expression in lung tissues from normal subjects ($n = 62$), stage I ($n = 21$), stage II ($n = 20$), stage III ($n = 14$) and stage IV ($n = 7$) of LUAD. The expression level of CD31 was evaluated by the microvascular density (MVD). (J−L) Correlation analyses between H2AC19 expression and VEGFA, CD31 and Ki-67 in all subjects ($n = 62$). (M) The survival analysis of the high and low-H2AC19 score groups stratified based on the median of H2AC19 staining scores calculated by OS prediction risk score formula. Data are expressed as mean ± SD and *n* indicates the number of biologically independent experiments. Two-tailed Student's unpaired t test analysis (H, I for CD31 and Ki67). One-way ANOVA followed by Tukey's post-test (I for H2AC19 and VEGFA). Spearman's correlations (J−L). $^{*}P < 0.05$, $^{**}P < 0.01$, $^{***}P < 0.001$.

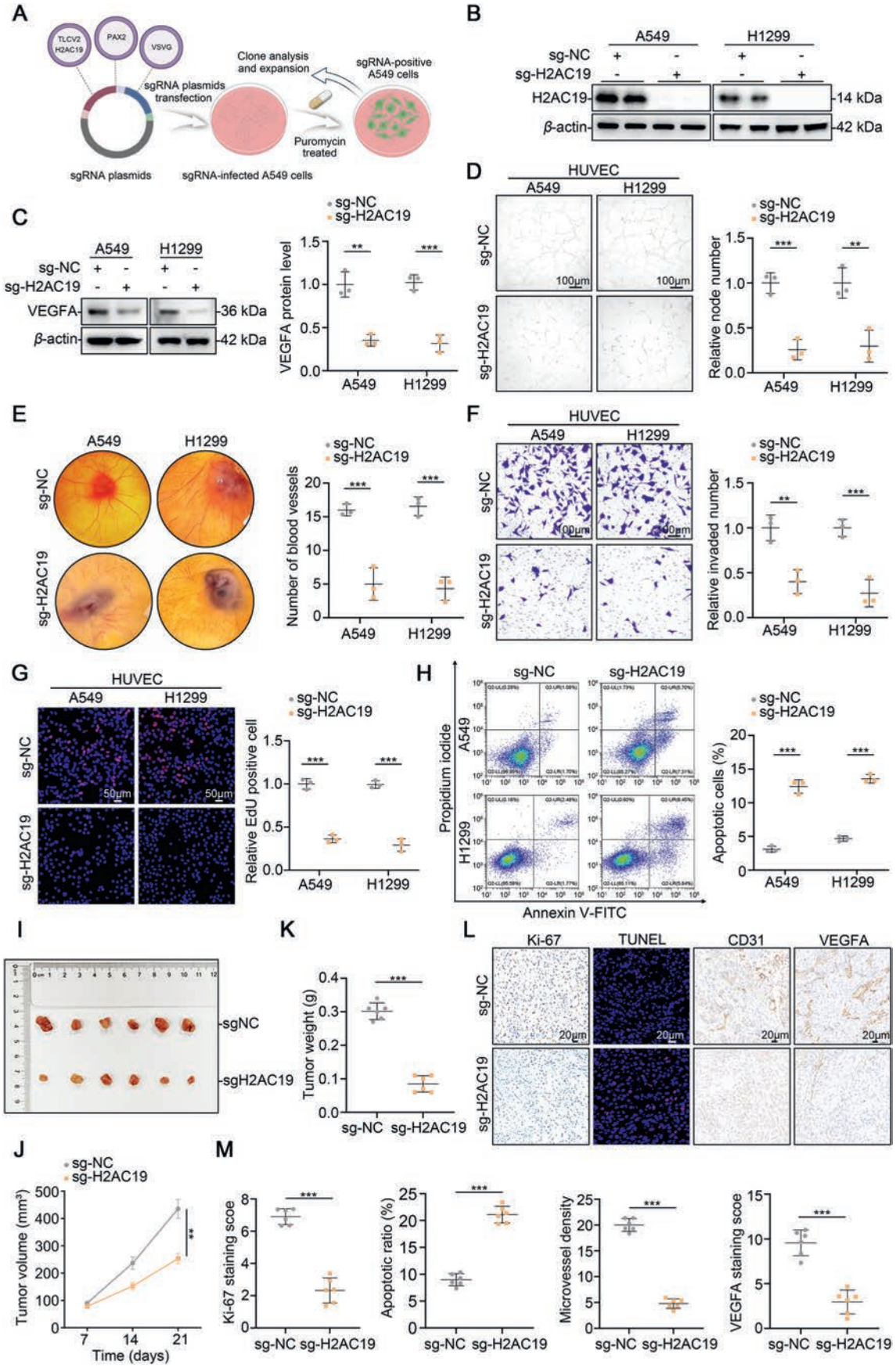
A
TLCV2 H2AC19
PAX2
VSVG
sgRNA plasmids transfection
Clone analysis and expansion
sgRNA-positive A549 cells
Puromycin treated
sgRNA plasmids
sgRNA-infected A549 cells
B
A549
H1299
sg-NC
sg-H2AC19
H2AC19
β-actin
14 kDa
42 kDa
C
VEGFA
36 kDa
VEGFA protein level
D
HUVEC
100μm
Relative node number
E
Number of blood vessels
F
Relative invaded number
G
50μm
Relative EdU positive cell
H
Propidium iodide
Annexin V-FITC
Apoptotic cells (%)
I
sgNC
sgH2AC19
K
Tumor weight (g)
L
Ki-67
TUNEL
CD31
VEGFA
20μm
J
Tumor volume (mm³)
Time (days)
M
Ki-67 staining scoe
Apoptotic ratio (%)
Microvessel density
VEGFA staining scoe

chambers to investigate their effects on capillary-like tube formation of HUVECs in Matrigel (Fig. 1F−H). Among several genes that exhibited inhibitory effects on tube formation, H2AC19 was the most prominent and was therefore selected for further investigation of its biological roles and underlying molecular mechanisms. Strikingly, the expression level of H2AC19 was markedly increased in LUAD patients with advanced clinical stages, augmented angiogenesis (validated by VEGFA and CD31 immunohistochemical staining), and accelerated tumor proliferation (confirmed by Ki67 labeling) (Fig. 1I). The information of the subjects in this study was summarized in Supporting Information Table S6. Importantly, the expression level of H2AC19 in LUAD patients was positively correlated with angiogenesis (Fig. 1J and K) and tumor progression (Fig. 1L). Kaplan-Meier survival curves revealed that LUAD patients with high H2AC19 expression exhibited shorter overall survival (Fig. 1M). Furthermore, univariate and multivariate Cox regression analyses demonstrated that H2AC19 expression served as an independent prognostic factor for overall survival of LUAD patients (Supporting Information Table S7). Taken together, these results indicate that elevated H2AC19 expression is a poor prognostic factor for LUAD. In addition, we further analyzed H2AC19 expression across clinically established molecular subtypes of LUAD. Within the TCGA-LUAD cohort, H2AC19 exhibited the highest expression levels in KRAS-mutant tumors compared with other driver mutation subtypes, including EGFR, BRAF, ALK, ROS1, MET, NRG, and RET mutants (Fig. S2L). Immunohistochemical validation further confirmed that KRAS-mutant tumors exhibited modestly higher H2AC19 protein levels than EGFR- or BRAF-mutant tumors (Fig. S2M). These observations suggest that the H2AC19-driven angiogenic pathway may be critical and functionally predominant in KRAS-mutant LUAD, a subtype that still lacks effective targeted therapeutic strategies.

3.3. H2AC19 knockout suppressed LUAD cell growth, migration and angiogenesis

To further elucidate the role of H2AC19 in LUAD, we generated H2AC19-deficient A549 and H1299 cell lines by using CRISPR/Cas9 editing system (Fig. 2A and B). We found that H2AC19 knockout in LUAD cells significantly reduced the expression (Fig. 2C) and secretion (Supporting Information Fig. S3A) levels of VEGFA. Using a co-culture system of LUAD cells and HUVECs, we found that H2AC19 deficiency in LUAD cells impaired the tube formation capacity (Fig. 2D and E), migratory ability (Fig. 2F) and proliferative activity (Fig. 2G) of HUVECs compared with their controls. Moreover, assessments *via* flow cytometry (Fig. 2H), colony formation assays (Fig. S3B) and wound-healing assays (Fig. S3C) demonstrated that H2AC19 knockout also significantly induced apoptosis, inhibited proliferation and migration of LUAD cells.

We then performed xenograft tumor-formation assays to evaluate the functions of H2AC19 in LUAD *in vivo*. The results showed that H2AC19 knockout cells exerted remarkable tumor-suppressive effects (Fig. 2I), with both the volume and weight of the derived tumors being significantly less than those of tumors from control cells (Fig. 2J and K). Immunohistochemistry staining and TdT-mediated dUTP Nick-End Labeling (TUNEL) assay revealed decreased Ki67 expression and increased apoptotic cells in the H2AC19 knockout group. Moreover, we explored the correlation between H2AC19 and angiogenesis *in vivo* and found that H2AC19 knockout also resulted in reduced VEGFA expression and decreased microvascular density (MVD) compared with the control group (Fig. 2L). Taken together, these findings demonstrate that H2AC19 knockout suppresses angiogenesis and tumor growth both *in vivo* and *in vitro*.

3.4. H2AC19 deficiency inhibits angiogenesis by downregulating the expression of MMP-1 in LUAD

To investigate the molecular mechanism by which H2AC19 promotes LUAD, we performed unbiased RNA-sequencing (RNA-seq) in A549 cells transduced with sg-H2AC19 or sg-NC, and screened for differentially expressed mRNAs. Kyoto Encyclopedia of Genes and Genomes (KEGG) and Gene Set Enrichment Analysis (GSEA) verified that H2AC19 was closely associated with angiogenesis-related signaling pathways (Fig. 3A−D). Among all differentially expressed genes, matrix metalloproteinase-1 (MMP-1) attracted our particular interest, as it showed the most significant fold change following H2AC19 knockout (Fig. 3E) and is known to play a pivotal role in angiogenesis and tumor progression[17]. We further confirmed that H2AC19 knockout decreased both the mRNA and protein levels of MMP-1 in LUAD cells (Fig. 3F and G).

To further determine whether MMP-1 is a key regulator linking H2AC19 and angiogenesis in LUAD, we generated H2AC19-overexpressing (Fig. 3H) and MMP-1-deficient (Supporting Information Fig. S4A) A549 and H1299 cells. It was found that knockout of MMP-1 in LUAD cells counteracted the effects of H2AC19 on VEGFA secretion (Fig. S4B), HUVEC tube formation (Fig. 3I and J), and migration and proliferation of HUVECs (Fig. S4C and S4D) and LUAD cells (Fig. S4E−S4G). Similar results were found in *in vivo* studies (Fig. 3K−N).

Figure 2 H2AC19 knockout decreased LUAD cell growth, migration, and angiogenesis. (A) Schematic overview of the CRISPR/Cas9 system in LUAD cells. (B) The knockout efficiency of H2AC19 in A549 and H1299 cells confirmed by Western blot analysis. (C) Western blot analysis of VEGFA protein levels in A549 and H1299 cells with different treatments. (D) Tube formation assay of HUVECs treated for 48 h with conditioned medium (CM) from A549 and H1299 cells under different conditions. Scale bar = 100 μm. (E) Representative images of blood vessels in chick chorioallantoic membrane (CAM) assay after treatment with different CM. (F) Transwell assay of HUVEC migration treated with CM from A549 and H1299 cells under different conditions. Scale bar = 100 μm. (G) The EDU assay of HUVEC proliferative treated with CM in A549 and H1299 cells under different conditions. Scale bar = 50 μm. (H) Flow cytometry analysis of apoptosis in A549 cells and H1299 cells. (I) Orthotopic tumor model in nude mice using A549 cells with stable H2AC19 knockout and their control. (J) Tumor volumes in the tumor-bearing mice measured at the indicated time points after cell implantation. (K) Tumor weights in the tumor-bearing mice measured after cell implantation. (L, M) TdT-mediated dUTP Nick-End labeling (TUNEL) assay and representative immunohistochemistry images of CD31, VEGFA and Ki67 expression from formalin-fixed paraffin-embedded xenograft sections. DAPI (4′,6-diamidino-2-phenylindole) was used as a nuclear staining. Scale bar = 20 μm. Data are expressed as mean ± SD and *n* indicates the number of biologically independent experiments. Two-tailed Student's unpaired *t* test analysis (C−H, J, K, M). $*P < 0.05$, $**P < 0.01$, $***P < 0.001$.

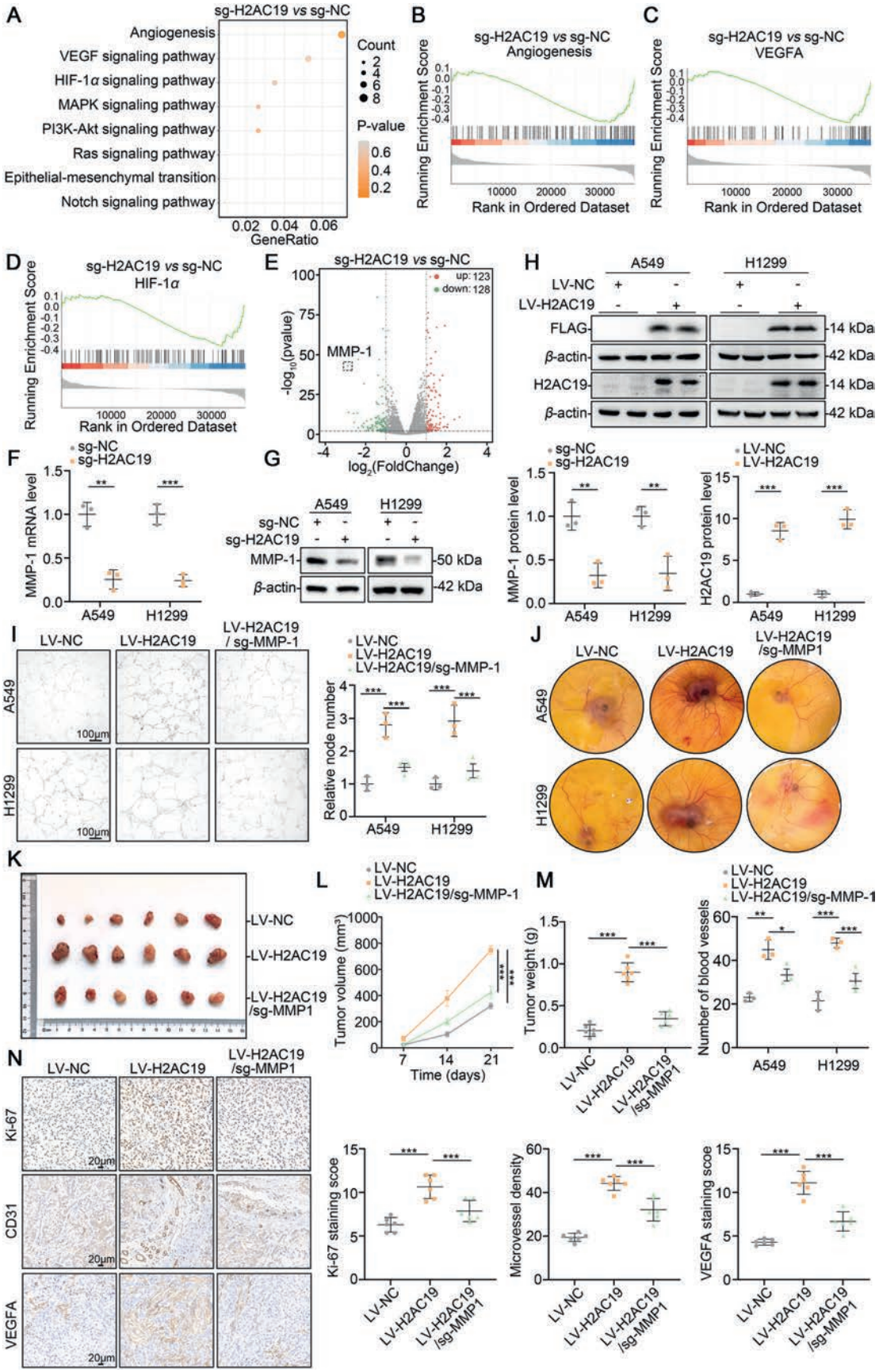

Figure 3 H2AC19 deficiency inhibits angiogenesis by downregulating expression of MMP-1 in LUAD. (A) Kyoto Encyclopedia of Genes and Genomes (KEGG) pathway enrichment based on the RNA-seq of A549 cells across different groups. (B–D) Gene Set Enrichment Analysis

3.5. H2AC19 promotes angiogenesis through the p300/EGR1/MMP-1 pathway in LUAD

Given that histone H2A variants function as molecular scaffolds for protein interactions and transcriptional regulation[18−22], we hypothesized that H2AC19 exerts its pro-angiogenic effects through interaction with transcriptional regulators. To test this, we performed protein-protein interaction prediction using the Search Tool for the Retrieval of Interacting Genes (STRING) database. Among the predicted interactors, the association between H2AC19 and the histone acetyltransferase p300 drew our attention due to its well-established role as a transcriptional co-activator and critical oncogenic driver[23,24] (Fig. 4A). It is known that p300 maintains gene expression programs primarily by lysine acetylation of histones, including lysine 4, 9, 14, 18 and 27 on histone 3 (H3K4, H3K9, H3K14, H3K18 and H3K27)[25]. We subsequently assessed p300-mediated histones acetylation in LUAD cells and found that H2AC19 bound to p300 (Fig. 4B), knockout of H2AC19 preferentially inhibited H3K27 acetylation without significantly affecting acetylation at other sites (Fig. 4C). Given the histone nature of H2AC19, we further conducted genome-wide chromatin immunoprecipitation (ChIP) -seq (Fig. 4D and Supporting Information Fig. S5A). Integrated analysis of ChIP-seq and RNA-seq datasets identified 65 candidate genes as direct downstream targets of H2AC19, seven of which genes were strongly associated with angiogenesis (Fig. 4E). Early growth response 1 (EGR1), the most markedly dysregulated gene among these candidates and a well-documented direct upstream regulator of MMP-1[26] exhibited a robust H2AC19 binding peak in the vicinity of its transcription start site within the promoter region, as verified by ChIP-seq (Fig. 4F) and ChIP-qPCR (Fig. S5B). Subsequent ChIP-qPCR assays revealed that H2AC19 knockout decreased p300 occupancy and H3K27 acetylation levels at the EGR1 promoter (Fig. 4G), whereas its overexpression increased the enrichment of both factors (Fig. S5C). H2AC19 knockout downregulated EGR1 expression at both mRNA and protein levels (Fig. 4H and Fig. S5D). Conversely, H2AC19 overexpression enhanced H3K27ac at the EGR1 promoter, upregulated EGR1 and MMP-1expression, and promoted angiogenesis and tumor progression. These effects were abolished by the p300 inhibitor A-485 (Fig. 4I, Fig. S5E−S5L) or EGR1 knockout (Supporting Information Fig. S6). Similar results were found *in vivo* (Supporting Information Fig. S7). These findings indicate that the H2AC19-p300 axis promotes EGR1 transcription through H3K27 acetylation. Rescue experiments confirmed that exogenous EGR1 (Supporting Information Fig. S8) or MMP-1 (Supporting Information Fig. S9) overexpression reversed the inhibitory effects of H2AC19 knockout on angiogenesis and tumor progression, demonstrating that H2AC19 functions through the EGR1/MMP-1 axis. In addition, we found that the levels of H3K27ac and EGR1 were significantly upregulated in LUAD patients (Fig. 4I), which was positively correlated with H2AC19 expression (Fig. 4J and K).

3.6. The H2AC19 deleted mutation of aa 24−88 counteracted the effects of H2AC19 on LUAD

To characterize the structural basis of the interaction between H2AC19 and p300, we employed AlphaFold 3 and Chimera X for structural modeling. The analysis revealed that H2AC19 and p300 share structural motifs that facilitate direct binding and form a defined protein interaction interface (Fig. 5A), consistent with the Predicted Aligned Error (PAE) analysis (Fig. 5B). To further map the binding region between H2AC19 and p300, we constructed three H2AC19 truncated mutants based on predictions from the UniProtKB/Swiss-Prot and Simple Modular Architecture Research Tool (SMART) databases, with deletion of amino acid (aa) 2−22 (Mut1), aa 24−88 (Mut2) or aa 92−126 (Mut3) (Fig. 5C). It was found that H2AC19 lacking the aa 24−88 fragment (Mut2) abolished binding to p300, whereas wild type (WT) and the other two mutations retained binding capability (Fig. 5D). Accordingly, Mut2 significantly reduced p300 occupancy and H3K27 acetylation at the EGR1 promoter compared to H2AC19-WT (Fig. 5E). In line with these findings, H2AC19-Mut2 decreased EGR1 and MMP-1 expression compared to H2AC19-WT (Fig. 5F). Functionally, Mut2 reversed H2AC19-induced angiogenesis, as evidenced by reduced tube formation, VEGFA levels, migration and proliferation of HUVECs (Fig. 5G−L), confirming that the aa 24−88 region is essential for H2AC19 binding to p300 and its pro-angiogenic function.

3.7. H2AC19 promotes angiogenesis and tumor progression in LUAD organoid models

To further verify the role of H2AC19 on angiogenesis in LUAD clinically, we established Patient-derived organoids (PDOs) to recapitulate the native features of primary LUAD (Fig. 6A). Morphological evaluation confirmed the successful construction of PDOs (Fig. 6B). Immunofluorescence (IF) analyses revealed robust expression of the tumor markers, Napsin A and TTF1 (Fig. 6C), validating the fidelity of the organoid models. Notably, H2AC19 knockout result in reduced PDO size (Fig. 6D), impaired angiogenic potential, decreased proliferative capacity (Fig. 6F), and increased apoptosis (Fig. 6E and F). Moreover, overexpression of H2AC19 enhanced angiogenesis and proliferation in organoids, which was reversed by treatment with A-485 (Fig. 6G and H).

(GSEA) showing enrichment of angiogenesis, VEGFA and HIF-1α pathways. (E) Volcano plot of differentially expressed genes identified by RNA-seq analysis between groups. (F, G) qPCR and Western blot analysis of MMP-1 mRNA and protein levels in A549 and H1299 cells with different treatments. (H) The overexpression efficiency of H2AC19 in A549 and H1299 cells confirmed by Western blot analysis. (I) Tube formation assay of HUVECs treated for 48 h with conditioned medium (CM) from A549 and H1299 cells under different conditions. Scale bar = 100 μm. (J) Representative images of blood vessels in CAM assay after treatment with different CM. (K) Orthotopic tumor model in nude mice using A549 cells with stable H2AC19 overexpression and MMP-1 knockout. (L) Tumor volumes in the tumor-bearing mice measured at the indicated time points after cell implantation. (M) Tumor weights in the tumor-bearing mice measured after cell implantation. (N) Representative immunohistochemistry images of CD31, VEGFA and Ki67 expression from formalin-fixed paraffin-embedded xenograft sections. Scale bar = 20 μm. Data are expressed as mean ± SD and *n* indicates the number of biologically independent experiments. Two-tailed Student's unpaired *t* test analysis (F−H). Two-way ANOVA followed by Tukey's post-test (I, J, L−N). $*P < 0.05$, $**P < 0.01$, $***P < 0.001$.

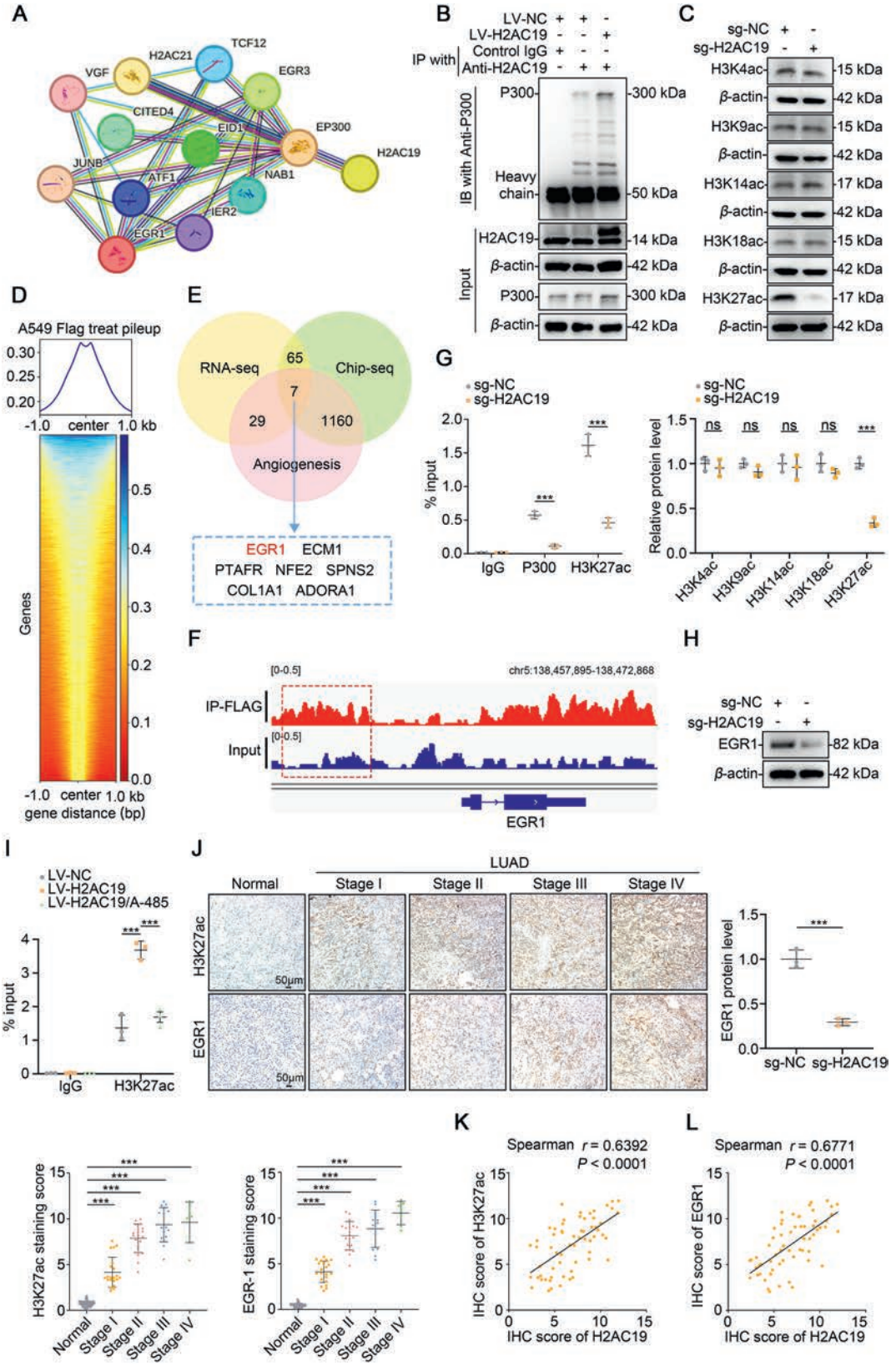

Figure 4 H2AC19 promotes angiogenesis through the p300/EGR1/MMP-1 pathway in LUAD. (A) Protein−protein interaction (PPI) networks based on Search Tool for the Retrieval of Interacting Genes (STRING) database. The line segment indicates both functional and physical protein associations. (B) Western blot analysis of p300 protein levels in A549 cells with different treatments. H2AC19 was immunoprecipitated with rabbit antibody to H2AC19 and the presence of p300 in the immune-complex was assessed by Western blot with the antibody to p300. Negative control using isotype matched normal IgG (rabbit) was done to check for antibody specificity. (C) Western blot analysis of the acetylation level of

3.8. Delivery of H2AC19-targeted siRNA using lipid nanoparticles for LUAD therapy

To evaluate the therapeutic potential of targeting H2AC19 in LUAD, we employed a previously reported lipid nanoparticle (LNP) formulation with favorable biosafety and high siRNA delivery efficiency to encapsulating H2AC19-targeting siRNA (si-H2AC19)[27,28]. The ionizable lipid-like material was synthesized and co-assembled with cholesterol and DMG-PEG2000 into LNPs *via* nanoprecipitation, followed by siRNA complexation (Fig. 7A−C). Dynamic light scattering (DLS) and transmission electron microscopy (TEM) confirmed that the LNP/siRNA complexes were uniformly spherical with a narrow size distribution (Fig. 7D), and the LNP/si-H2AC19 complexes effectively knocked down H2AC19 expression in LUAD cells (Supporting Information Fig. S10A), while markedly suppress angiogenesis and tumor progression (Fig. 7E, F and Fig. S10B−S10F). To further assess the *in vivo* antitumor efficacy of LNP/si-H2AC19, we administered the LNP/siRNA complexes *via* intratumorally injection into LUAD xenograft models (Fig. 7G). Notably, LNP/si-H2AC19 treatment significantly suppressed tumor growth and angiogenesis (Fig. 7H−K), supporting H2AC19 as a potential therapeutic target for LUAD.

4. Discussion

Despite considerable advances in diagnostic and therapeutic approaches for LUAD, the persistent challenges of poor prognosis and treatment resistance underscore the critical need for more precise prognostic tools. Angiogenesis, an essential prerequisite for tumor growth and metastasis, is a well-recognized hallmark of LUAD[29]. Hypoxia acts as a critical upstream driver by inducing pro-angiogenic gene expression, thereby promoting tumor invasion and metastasis and ultimately exacerbating patient prognosis[30,31]. In this study, we established a systematic approach to identify clinically valuable biomarkers by constructing a prognostic risk model based on hypoxia and angiogenesis-associated genes in LUAD. Notably, our model exhibited superior predictive accuracy compared with existing hypoxia and angiogenesis-related signatures, with particularly robust performance in long-term prognosis evaluation, highlighting its potential for clinical risk stratification and individualized prognostic assessment in LUAD patients.

Recent progress has shed light on how mutations, transcriptional deregulation and altered deposition machineries of histone variants modulate the process of tumorigenesis and angiogenesis[8]. Accumulating evidence has indicated that the histone H2A family plays indispensable roles in a variety of physiological and pathological processes, including tumorigenesis, yet their biological functions in the LUAD remain largely unexplored[9,32,33]. Among the 12 candidate genes from our prognosis risk model, we identified H2AC19, a relatively uncharacterized histone H2A variant[11−13], which emerged as the top candidate due to its marked upregulation in tumor tissues and strong correlation with aggressive disease features and poor prognosis in LUAD patients. CRISPR/Cas9-mediated genetic ablation of H2AC19 effectively suppressed tumor angiogenesis and progress in both *in vitro* and *in vivo* studies. Importantly, these findings were validated with clinical relevance in patient-derived organoids (PDOs), models that faithfully replicate the pathological and molecular attributes of native tumors[34,35]. These results not only extend the functional link between histone variants and tumor angiogenesis but also highlight the dual potential of H2AC19 as both a prognostic biomarker and a therapeutic target in the clinical management of LUAD.

To elucidate the mechanism by which H2AC19 regulates angiogenesis, we performed transcriptome sequencing following H2AC19 knockdown and identified matrix metalloproteinase1 (MMP1), a member of MMPs family as the most significantly downregulated gene. The elevated expression of multiple MMP family members in tumor tissues and its positive correlation with tumor progression have been well established for several decades[36−38]. Accumulating evidence has demonstrated that MMPs drive tumor angiogenesis by degrading the extracellular matrix, thereby promoting endothelial cell migration and activation, and ultimately supporting tumor growth and metastasis[39]. This functional role is consistent with the results of our sequencing experiments, thus confirming that MMP1 serves as a key downstream effector molecular mediating H2AC19-regulated angiogenic program.

In light of this discovery, we shifted our focus to elucidating the molecular mechanisms by which H2AC19 regulates the expression of MMP1 and other pro-angiogenetic genes. Given that H2A family variants may act as scaffolds for recruiting protein/DNA complexes, transcriptional regulation platforms, and heterochromatin silencers[18−22], we speculated that H2AC19 might exert its function through mediating protein−protein interactions (PPI). Through screening *via* the STRING database, we identified a strong predicted association between H2AC19 and the histone acetyltransferase p300, a prominent transcriptional co-activator[40], which was subsequently confirmed by co-immunoprecipitation.

Epigenetic dysregulation, particularly aberrant histone modification, is now recognized as a fundamental hallmark of multiple human malignancies, including LUAD[41−43]. Among these modifications, histone acetylation serves as a key activating marker associated to open chromatin and active regulatory elements[44]. The acetyltransferase p300, the major "writer" of this mark, is frequently overexpressed or hyperactivated in LUAD, thereby promoting oncogenic transcription programs[45,46]. Crucially, we

H3K4, H3K9, H3K14, H3K18 and H3K27 in A549 cells with different treatments. (D) ChIP-seq analysis of H2AC19 occupancy in A549 cells using FLAG-H2AC19 antibody. Profile diagram and heatmap showing H2AC19 signal distribution across ±1 kb of gene transcription start site (TSS). (E) Venn diagram showing the intersection of differentially expressed genes in RNA sequencing and CHIP sequencing with angiogenesis, including EGR1, ECM1, SPNS2, PTAFR, NFE2, ADORA1 and COL1A1. (F) ChIP-seq results showing the binding peak in the promoter region close to the TSS of EGR1. (G) ChIP-qPCR assay depicting the enrichments of p300 and H3K27ac at the EGR1 promoter in A549 cells. (H) Western blot analysis of EGR1 protein levels in A549 cells with different treatments. (I) ChIP-qPCR assay depicting the enrichments of H3K27ac at the EGR1 promoter in A549 cells. (J) Representative immunohistochemistry images of H3K27ac and EGR1 expression in lung tissues from normal subjects ($n = 62$), stage I ($n = 21$), stage II ($n = 20$), stage III ($n = 14$) and stage IV ($n = 7$) of LUAD. (K, L) Correlation analyses between H2AC19 expression and H3K27ac and EGR1 in all subjects ($n = 62$). Data are expressed as mean ± SD and n indicates the number of biologically independent experiments. Two-tailed Student's unpaired *t* test analysis (C, G, H). One-way ANOVA followed by Tukey's post-test (J). Two-way ANOVA followed by Tukey's post-test (I). Spearman's correlations (K, L). $*P < 0.05$, $**P < 0.01$, $***P < 0.001$.

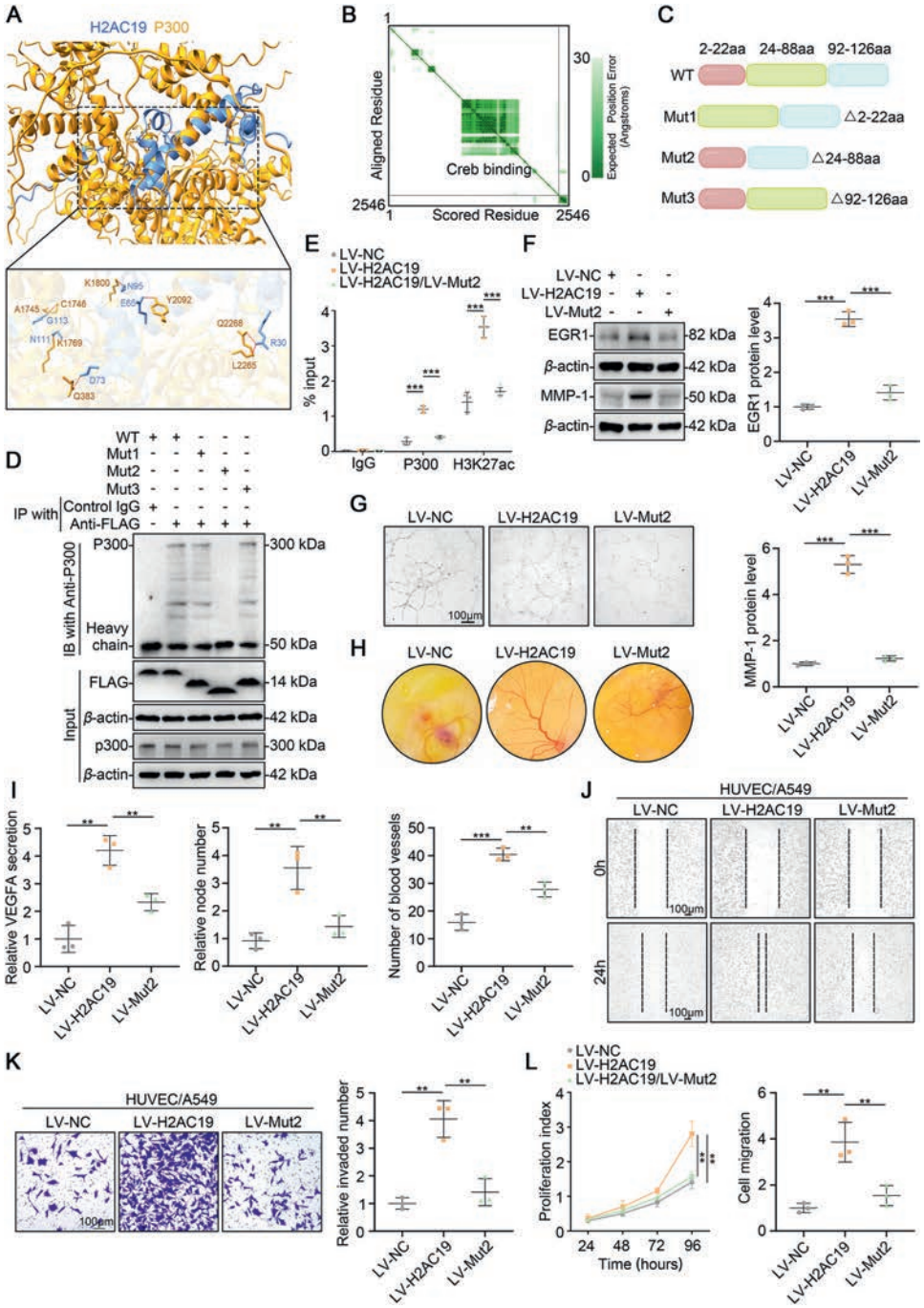

Figure 5 The H2AC19 Δaa24−88 mutation counteracted the effects of H2AC19 on LUAD. (A) H2AC19-P300 interaction analysis predicted by AlphaFold3. (B) Interactive 2D plot of Predicted Aligned Error (PAE) of H2AC19 and P300. (C) Three truncated mutants generated based on domain predictions from SMART and UniProtKB/Swiss-Prot databases: Mut1 (Δ2−22, low complexity region), Mut2 (Δ24−88, core domain), and Mut3 (Δ92−126, C-terminal region). (D) Western blot analysis of P300 protein levels in A549 cells with different treatments. FLAG-H2AC19 was immunoprecipitated with the rabbit antibody to FLAG and the presence of P300 in the immune-complex was assessed by Western blot with the antibody to P300. Negative control using isotype matched normal IgG (rabbit) was done to check for antibody specificity. (E) ChIP-qPCR assay depicting the enrichments of p300 and H3K27ac at the EGR1 promoter in A549 cells. (F) Western blot analysis of EGR1 and MMP-1 protein levels in A549 cells with different treatments. (G) Tube formation assay of HUVECs treated for 48 h with CM from A549 cells under different conditions. Scale bar = 100 μm. (H) Representative images of blood vessels in CAM assay after treatment with different CM. (I) Culture supernatant VEGFA levels determined by ELISA in A549 cells with different treatments. (J) Wound healing assay of HUVEC migration treated with CM from A549 cells under different conditions. Scale bar = 100 μm. (K) Transwell assay of HUVEC migration treated with CM from A549 cells under different conditions. Scale bar = 100 μm. (L) CCK-8 assay of HUVEC proliferation treated with conditioned medium (CM) from A549 cells under different conditions. Data are expressed as mean ± SD and *n* indicates the number of biologically independent experiments. Two-way ANOVA followed by Tukey's post-test (E−L). $^{*}P < 0.05$, $^{**}P < 0.01$, $^{***}P < 0.001$.

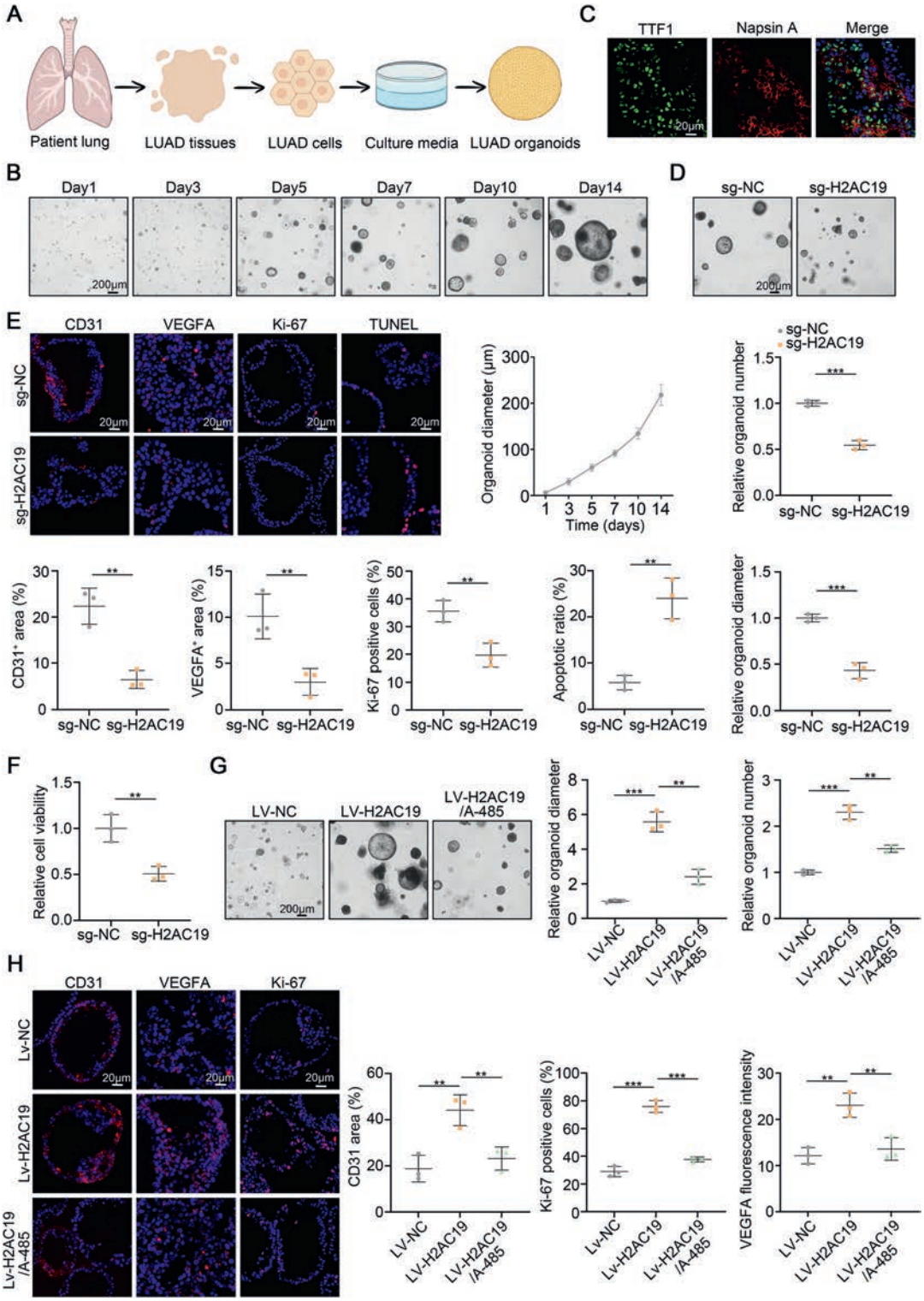

Figure 6 H2AC19 promotes angiogenesis and tumor progression in LUAD organoid models. (A) Schematic diagram of organoids construction of lung adenocarcinoma. (B) Bright-field images and growth curves of diameters from organoids in different time points. (C) Representative immunofluorescence images of TTF1 (green) and Napsin A (red) of patient-derived organoids (PDOs). DAPI was used as a nuclear staining. (D) Representative images of the numbers and diameter in organoids from different groups. (E) TUNEL assay and representative immunofluorescence images of Ki67, CD31 and VEGFA expression in organoids from different groups. DAPI was used as a nuclear staining. (F) CCK-8 assay of proliferation in organoids from different groups. (G) Representative images of the numbers and diameter in organoids from different groups. (H) Representative immunofluorescence images of CD31, VEGFA and Ki-67 in organoids from different groups. DAPI was used as a nuclear staining. Data are expressed as mean ± SD and n indicates the number of biologically independent experiments. Two-tailed Student's unpaired t test analysis (D−F). Two-way ANOVA followed by Tukey's post-test (G, H). $^{*}P < 0.05$, $^{**}P < 0.01$, $^{***}P < 0.001$.

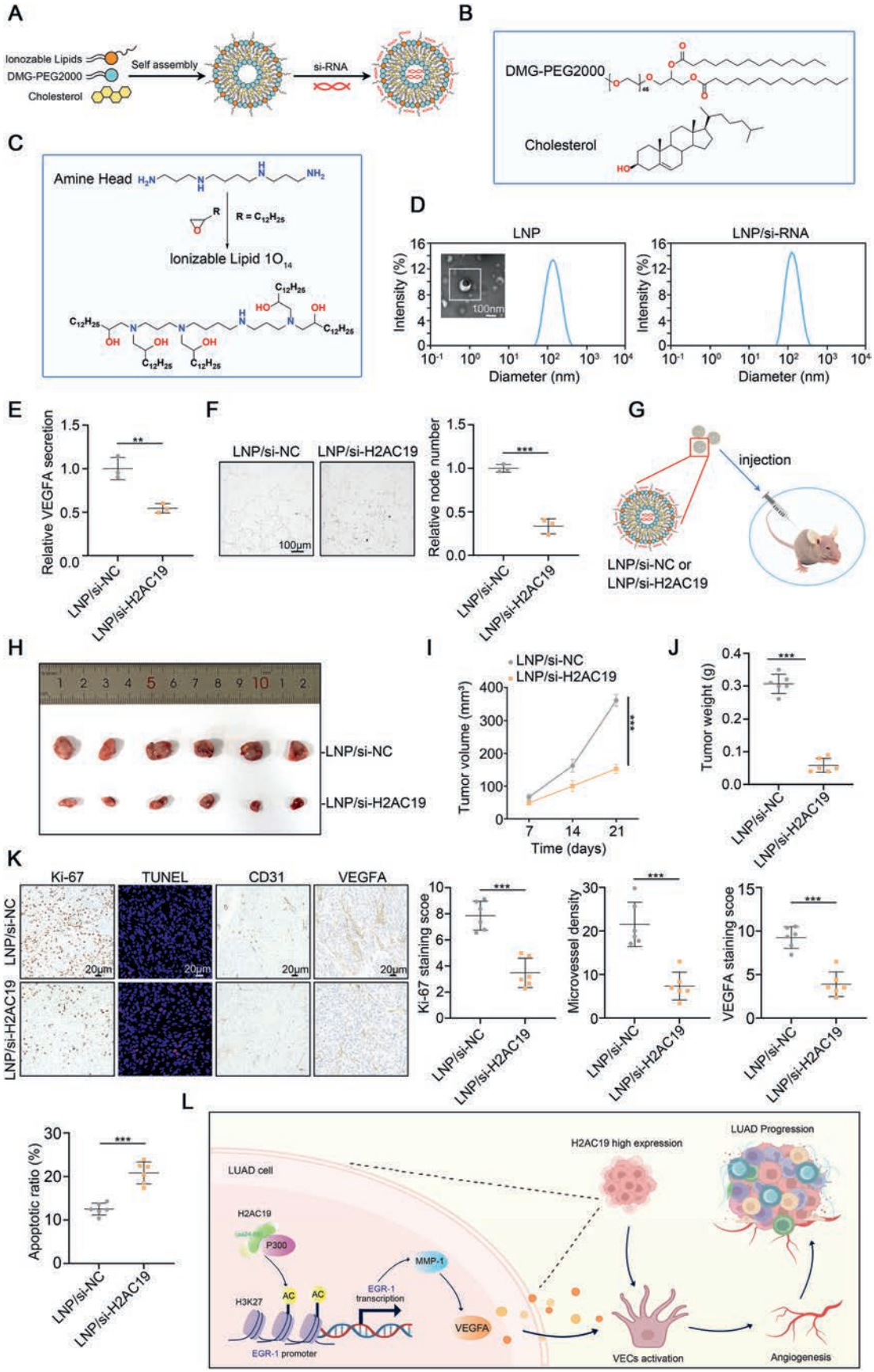
A
Ionozable Lipids
DMG-PEG2000
Cholesterol
Self assembly
si-RNA
B
DMG-PEG2000
Cholesterol
C
Amine Head
R = C12H25
Ionizable Lipid 1O14
D
LNP
LNP/si-RNA
Intensity (%)
Diameter (nm)
100nm
E
Relative VEGFA secretion
LNP/si-NC
LNP/si-H2AC19
F
LNP/si-NC
LNP/si-H2AC19
100μm
Relative node number
G
injection
LNP/si-NC or
LNP/si-H2AC19
H
LNP/si-NC
LNP/si-H2AC19
I
LNP/si-NC
LNP/si-H2AC19
Tumor volume (mm³)
Time (days)
J
Tumor weight (g)
K
Ki-67
TUNEL
CD31
VEGFA
20μm
Ki-67 staining score
Microvessel density
VEGFA staining score
L
Apoptotic ratio (%)
LUAD cell
H2AC19
P300
H3K27
AC
EGR-1 transcription
EGR-1 promoter
MMP-1
VEGFA
H2AC19 high expression
LUAD Progression
VECs activation
Angiogenesis

found that H2AC19 specifically regulates H3K27ac levels in LUAD without affecting other acetylation sites, suggesting that H2AC19 functions by recruiting p300 to specific genomic loci rather than by enhancing its global enzymatic activity. To identify the downstream transcriptional effectors of the H2AC19/p300 axis, we performed an integrated analysis of ChIP-seq and RNA-seq datasets. This analysis identified the transcription factor EGR1 as the top candidate, as evidenced by the presence of a strong H2AC19-binding peak near its transcription start site (TSS) and its significant downregulation following H2AC19 knockout. This finding is of considerable significance, as EGR1 is not only a reported promoter of LUAD cell proliferation, migration, and invasion[47], but also a potent regulator of angiogenesis that can activate key pro-angiogenic factors like MMP-1 and VEGFA[48,49]. These results directly link the epigenetic regulation of the H2AC19/p300 axis to the execution of specific pro-tumorigenic gene programs. Using ChIP-qPCR assays, we further confirmed that both H2AC19 and p300 are significantly enriched at the EGR1 promoter region, indicating that H2AC19 recruits p300 to enhance H3K27 acetylation at the EGR1 promoter region, thereby driving EGR1 transcriptional activation and subsequently facilitating MMP-1-mediated angiogenesis and progression of LUAD. Furthermore, the H2AC19 deletion mutant (Δ24−88) markedly reduced p300 occupancy at this locus, consequently abrogating H2AC19-mediated promotion of angiogenesis and LUAD progression. These findings establish that residues 24−88 are indispensable for H2AC19 function, consistent with its structural homology to canonical H2A variants in mediating nucleosome assembly, chromatin remodeling and protein−protein interactions[8,33,50,51].

It should be noted that although anti-angiogenic therapies targeting the VEGF signaling pathway are commonly used strategies in the treatment of LUAD in clinical practice, their long-term efficacy is often limited by acquired resistance, which is likely attributable to the compensatory activation of alternative pro-angiogenic signaling pathways following VEGFA blockade[52−55]. This challenge underscores the critical need to identify and target upstream regulators of angiogenesis that can modulate this process at its origin or *via* multiple downstream effectors. Building upon our findings that H2AC19 promotes tumor angiogenesis, we have initiated exploratory efforts to develop therapeutic agents targeting this new regulator. Preliminary data demonstrate that liposome-encapsulated H2AC19-targeted siRNA effectively blocks H2AC19 expression and suppresses tumor angiogenesis and progression, positioning a promising direction for future therapeutic development in LUAD.

Collectively, our study defines a complete signaling axis whereby H2AC19 binds to p300 *via* its amino acid residues 24−88, recruits p300 to the EGR1 promoter region, promotes H3K27 acetylation, and thereby leads to the upregulation of MMP-1 expression to drive angiogenesis and LUAD progression (Fig. 7L).

Further studies are warranted to address the limitations of this work. Although we have established a pro-angiogenic role for H2AC19 in LUAD, the precise upstream regulators controlling its expression within the tumor microenvironment require further investigation. Moreover, despite the identification of the p300/EGR1/MMP1 pathway as a key mechanism, a comprehensive dissection of additional H2AC19 downstream targets will be necessary to fully delineate its functional network. Finally, and most importantly, while preliminary efforts have been made towards developing drugs that target the H2AC19 pathway, we recognize that there remains a long way to go before meeting the requirements for a promising therapeutic agent.

5. Conclusions

Taken together, this study identifies histone variant H2AC19 as a key epigenetic regulator in LUAD progression, at least in part through the p300/EGR1/MMP-1 signaling pathway. Genetic or pharmacological targeting of H2AC19 at multiple levels may provide a promising therapeutic strategy for the antiangiogenic intervention of LUAD.

Acknowledgments

This study was supported by the Shandong Provincial Natural Science Foundation of China (ZR2025QC1660), the National Nature Science Foundation of China (82470767) and the Shandong University Foundation (6010122034).

Author contributions

Fuwen Zuo conducted the *in vivo* and *in vitro* experiments, performed the data analysis, and helped write the manuscript. Jinlong Yu, Xiaorui Liu and Tong Liu contributed to the experimental design and performed the *in vitro* experiments. Jilong Yin and Yuhan Pang performed the *in vivo* animal studies. Pengzhong Ding helped with the LNP and performed the data analyses and visualization. Zhengdong Luo, Xiaofeng Wang and Shuang Qi helped design the experiments. Lutao Du, Ling Guo and Yirong Zhang analyzed the clinical data. Fan Yi, Xiaoshi Zhang and Ziying Wang designed the experiments, interpreted the data, wrote the manuscript, and approved the final version of the manuscript for publication.

Figure 7 Delivery of H2AC19-targeted siRNA using lipid nanoparticles for LUAD therapy. (A) Schematic diagram of lipid nanoparticles (LNP)-mediated siRNA delivery. (B) The chemical structure of DMG-PEG2000 and Cholesterol. (C) The ionizable lipids synthesized by ring-opening reaction between epoxide and amine-containing molecules. (D) Size distribution and morphology of 1O14-LNP obtained by Dynamic light scattering (DLS) and transmission electron microscopy. (TEM). (E) Culture supernatant VEGFA levels were determined by ELISA in A549 cells with different treatments. (F) Tube formation assay of HUVECs treated for 48 h with conditioned medium (CM) from A549 cells under different conditions. Scale bar = 100 μm. (G) The schematic diagram of LNP mediated siRNA delivery for LUAD treatment. (H) Orthotopic tumor model in nude mice using A549 cells with LNP/si-RNA treatments. (I) Tumor volumes in the tumor-bearing mice measured at the indicated time points after cell implantation. (J) Tumor weights in the tumor-bearing mice measured after cell implantation. (K) TUNEL assay and representative immunohistochemistry images of CD31, VEGFA and Ki67 expression from formalin-fixed paraffin-embedded xenograft sections. Scale bar = 20 μm. (L) Schematic depicting H2AC19 promotes angiogenesis by regulating p300/EGR1/MMP-1 axis in LUAD. Data are expressed as mean ± SD and *n* indicates the number of biologically independent experiments. Two-tailed Student's unpaired *t* test analysis (E, F, I−K). $*P < 0.05$, $**P < 0.01$, $***P < 0.001$.

Conflicts of interest

All the authors declared no competing interests.

Appendix A. Supporting information

Supporting information to this article can be found online at https://doi.org/10.1016/j.apsb.2026.07.010.

References

1. Siegel RL, Giaquinto AN, Jemal A. Cancer statistics, 2024. *CA Cancer J Clin* 2024;**74**:12−49.
2. Sung H, Ferlay J, Siegel RL, Laversanne M, Soerjomataram I, Jemal A, et al. Global Cancer Statistics 2020: GLOBOCAN estimates of incidence and mortality worldwide for 36 cancers in 185 countries. *CA Cancer J Clin* 2021;**71**:209−49.
3. Leiter A, Veluswamy RR, Wisnivesky JP. The global burden of lung cancer: current status and future trends. *Nat Rev Clin Oncol* 2023;**20**:624−39.
4. Tan N, Li Y, Ying J, Chen W. Histological transformation in lung adenocarcinoma: insights of mechanisms and therapeutic windows. *J Transl Int Med* 2024;**12**:452−65.
5. Ge T, Gu X, Jia R, Ge S, Chai P, Zhuang A, et al. Crosstalk between metabolic reprogramming and epigenetics in cancer: updates on mechanisms and therapeutic opportunities. *Cancer Commun* 2022;**42**: 1049−82.
6. Wong LH, Tremethick DJ. Multifunctional histone variants in genome function. *Nat Rev Genet* 2025;**26**:82−104.
7. Maze I, Noh KM, Soshnev AA, Allis CD. Every amino acid matters: essential contributions of histone variants to mammalian development and disease. *Nat Rev Genet* 2014;**15**:259−71.
8. Buschbeck M, Hake SB. Variants of core histones and their roles in cell fate decisions, development and cancer. *Nat Rev Mol Cell Biol* 2017;**18**:299−314.
9. Martire S, Banaszynski LA. The roles of histone variants in fine-tuning chromatin organization and function. *Nat Rev Mol Cell Biol* 2020;**21**:522−41.
10. Ghiraldini FG, Filipescu D, Bernstein E. Solid tumours hijack the histone variant network. *Nat Rev Cancer* 2021;**21**:257−75.
11. Groysman L, Carlsen L, Huntington KE, Shen WH, Zhou L, El-Deiry WS. Chemotherapy-induced cytokines and prognostic gene signatures vary across breast and colorectal cancer. *Am J Cancer Res* 2021;**11**:6086−106.
12. Zheng B, Fu M, Lou F, He Y, Zhao L, Haung X, et al. Claudin18.2 promote gastric cancer proliferation by activating MCM2/5. *Sci Rep* 2026;**16**:10263.
13. Zhang X, Zhai Y, Zhang D, Che C, Zhang Y, Li Q, et al. RNAseq analysis of the drug jian-yan-ling (JYL) using both *in vivo* and *in vitro* models. *Heliyon* 2023;**9**:e16143.
14. Dijkstra KK, Vendramin R, Karagianni D, Witsen M, Gálvez-Cancino F, Hill M, et al. Subclonal immune evasion in non-small cell lung cancer. *Cancer Cell* 2025;**43**:1833−49.
15. Zijlstra A, Lewis J, Degryse B, Stuhlmann H, Quigley JP. The inhibition of tumor cell intravasation and subsequent metastasis *via* regulation of *in vivo* tumor cell motility by the tetraspanin CD151. *Cancer Cell* 2008;**13**:221−34.
16. Yang M, Mu Y, Yu X, Gao D, Zhang W, Li Y, et al. Survival strategies: how tumor hypoxia microenvironment orchestrates angiogenesis. *Biomed Pharmacother* 2024;**176**:116783.
17. Michael M, Babic B, Khokha R, Tsao M, Ho J, Pintilie M, et al. Expression and prognostic significance of metalloproteinases and their tissue inhibitors in patients with small-cell lung cancer. *J Clin Oncol* 1999;**17**:1802−8.
18. Li Q, Zhao C, Guo Y, Bai Y, Liu J, Jin X, et al. Direct recruitment of TONSOKU by the N-terminal tails of histone variants H2A.X and H2A.W coordinates DNA repair. *Sci Adv* 2025;**11**:eady2104.
19. Stucki M, Clapperton JA, Mohammad D, Yaffe MB, Smerdon SJ, Jackson SP. MDC1 directly binds phosphorylated histone H2AX to regulate cellular responses to DNA double-strand breaks. *Cell* 2005; **123**:1213−26.
20. Jiang H, Zhao M, Liu M, Zhang W, Xu J, Pélissier T, et al. H3 acetylation triggers SWR1 recruitment to promote H2A.Z incorporation into chromatin and stimulate gene expression. *Plant Physiol* 2025; **199**:kiaf469.
21. Zhang H, Roberts DN, Cairns BR. Genome-wide dynamics of Htz1, a histone H2A variant that poises repressed/basal promoters for activation through histone loss. *Cell* 2005;**123**:219−31.
22. Cantariño N, Douet J, Buschbeck M. MacroH2A−an epigenetic regulator of cancer. *Cancer Lett* 2013;**336**:247−52.
23. Hogg SJ, Motorna O, Cluse LA, Johanson TM, Coughlan HD, Raviram R, et al. Targeting histone acetylation dynamics and oncogenic transcription by catalytic P300/CBP inhibition. *Mol Cell* 2021;**81**:2183−200.
24. Wang J, Yu X, Gong W, Liu X, Park KS, Ma A, et al. EZH2 non-canonically binds cMyc and p300 through a cryptic transactivation domain to mediate gene activation and promote oncogenesis. *Nat Cell Biol* 2022;**24**:384−99.
25. Shvedunova M, Akhtar A. Modulation of cellular processes by histone and non-histone protein acetylation. *Nat Rev Mol Cell Biol* 2022;**23**: 329−49.
26. Wang B, Guo H, Yu H, Chen Y, Xu H, Zhao G. The role of the transcription factor EGR1 in cancer. *Front Oncol* 2021;**11**:642547.
27. Sun K, Gong L, Liu J, Liu Y, Li Y, Zhang J, et al. LINC 02086, a novel biomarker for early detection of gastric cancer and a target for cancer therapy. *Cell Death Differ* 2026;**33**:798−812.
28. Zhang H, Ding F, Zhu Z, Sun Q, Yang C. Engineered ionizable lipid nanoparticles mediated efficient siRNA delivery to macrophages for anti-inflammatory treatment of acute liver injury. *Int J Pharm* 2023; **631**:122489.
29. Goel HL, Mercurio AM. VEGF targets the tumour cell. *Nat Rev Cancer* 2013;**13**:871−82.
30. Keith B, Simon MC. Hypoxia-inducible factors, stem cells, and cancer. *Cell* 2007;**129**:465−72.
31. Semenza GL. Hypoxia-inducible factors: mediators of cancer progression and targets for cancer th erapy. *Trends Pharmacol Sci* 2012; **33**:207−14.
32. Lai PM, Chan KM. Roles of histone H2A variants in cancer development, prognosis, and treatment. *Int J Mol Sci* 2024;**25**:3144.
33. Talbert PB, Henikoff S. Histone variants at a glance. *J Cell Sci* 2021; **134**:jcs244749.
34. Tong L, Cui W, Zhang B, Fonseca P, Zhao Q, Zhang P, et al. Patient-derived organoids in precision cancer medicine. *Med* 2024;**5**:1351−77.
35. Wu W, Li X, Yu S. Patient-derived tumour organoids: a bridge between cancer biology and personalised therapy. *Acta Biomater* 2022; **146**:23−36.
36. Stetler-Stevenson WG. Matrix metalloproteinases in angiogenesis: a moving target for therapeutic intervention. *J Clin Investig* 1999;**103**: 1237−41.
37. Hiraoka N, Allen E, Apel IJ, Gyetko MR, Weiss SJ. Matrix metalloproteinases regulate neovascularization by acting as pericellular fibrinolysins. *Cell* 1998;**95**:365−77.
38. Zucker S, Cao J, Chen WT. Critical appraisal of the use of matrix metalloproteinase inhibitors in cancer treatment. *Oncogene* 2000;**19**: 6642−50.
39. Deryugina EI, Quigley JP. Tumor angiogenesis: MMP-mediated induction of intravasation- and metastasis-sustaining neovasculature. *Matrix Biol* 2015;**44-46**:94−112.
40. Ortega E, Rengachari S, Ibrahim Z, Hoghoughi N, Gaucher J, Holehouse AS, et al. Transcription factor dimerization activates the p300 acetyltransferase. *Nature* 2018;**562**:538−44.
41. Hanahan D. Hallmarks of cancer: new dimensions. *Cancer Discov* 2022;**12**:31−46.
42. Hogg SJ, Beavis PA, Dawson MA, Johnstone RW. Targeting the epigenetic regulation of antitumour immunity. *Nat Rev Drug Discov* 2020;**19**:776−800.

43. Dawson MA, Kouzarides T. Cancer epigenetics: from mechanism to therapy. *Cell* 2012;**150**:12−27.
44. Bajbouj K, Al-Ali A, Ramakrishnan RK, Saber-Ayad M, Hamid Q. Histone modification in NSCLC: molecular mechanisms and therapeutic targets. *Int J Mol Sci* 2021;**22**:11701.
45. Zhang T, Xia W, Song X, Mao Q, Huang X, Chen B, et al. Super-enhancer hijacking LINC01977 promotes malignancy of early-stage lung adenocarcinoma addicted to the canonical TGF-β/SMAD3 pathway. *J Hematol Oncol* 2022;**15**:114.
46. Tao J, Bian X, Zhou J, Zhang M. From microscopes to molecules: the evolution of prostate cancer diagnostics. *CytoJournal* 2024;**21**:29.
47. Ferraro B, Bepler G, Sharma S, Cantor A, Haura EB. EGR1 predicts PTEN and survival in patients with non-small-cell lung cancer. *J Clin Oncol* 2005;**23**:1921−6.
48. Kim JH, Choi DS, Lee OH, Oh SH, Lippman SM, Lee HY. Anti-angiogenic antitumor activities of IGFBP-3 are mediated by IGF-independent suppression of Erk1/2 activation and Egr-1-mediated transcriptional events. *Blood* 2011;**118**:2622−31.
49. Sang QX. Complex role of matrix metalloproteinases in angiogenesis. *Cell Res* 1998;**8**:171−7.
50. Suto RK, Clarkson MJ, Tremethick DJ, Luger K. Crystal structure of a nucleosome core particle containing the variant histone H2A.Z. *Nat Struct Biol* 2000;**7**:1121−4.
51. Osakabe A, Lorkovic ZJ, Kobayashi W, Tachiwana H, Yelagandula R, Kurumizaka H, et al. Histone H2A variants confer specific properties to nucleosomes and impact on chromatin accessibility. *Nucleic Acids Res* 2018;**46**:7675−85.
52. Guelfi S, Hodivala-Dilke K, Bergers G. Targeting the tumour vasculature: from vessel destruction to promotion. *Nat Rev Cancer* 2024;**24**:655−75.
53. Itatani Y, Kawada K, Yamamoto T, Sakai Y. Resistance to anti-angiogenic therapy in cancer-alterations to anti-VEGF pathway. *Int J Mol Sci* 2018;**19**:1232.
54. Jayson GC, Kerbel R, Ellis LM, Harris AL. Antiangiogenic therapy in oncology: current status and future directions. *Lancet* 2016;**388**:518−29.
55. Wang R, Zhang R, Zhou J, Ran J. Crosstalk between anti-angiogenic and pro-angiogenic pathways in disease: mechanisms and therapeutic strategies. *Pharmacol Ther* 2025;**276**:108934.